

**INTRODUCTION OF FOREIGN METALS ONTO UNSUPPORTED AND
SUPPORTED NICKEL PRASEODYMIUM OXIDE CATALYST FOR
CONVERSION OF CARBON DIOXIDE TO METHANE**

FARIDAH BINTI MOHD MARSIN

UNIVERSITI TEKNOLOGI MALAYSIA

**To my beloved father and mother
And all the special people in my life
that made me live my life to the fullest**

ACKNOWLEDGEMENTS

First and foremost, in a humble way I wish to give all the Praise to Allah, the Almighty God for His mercy has given me the strength, *His blessings* and enough time to complete this work.

My greatest gratitude goes to my supervisor, Assoc Prof Dr. Nor Aziah Buang, for the brilliant ideas, suggestions, helpful guidance, and for tolerating with all the mischievous behavior I showed and imparting her vast knowledge to me. Her constant advice on writing up the thesis made this report a remarkable success.

Sincere appreciation also goes to all who have helped in this research, Prof. Dr. Wan Azelee Wan Abu Bakar for his wise and useful ideas, Assoc. Prof Dr Yusuf Othman for financial support and his sincere help in carrying out my research, Prof. Zakaria Mohd Amin (Universiti Sains Malaysia), Mrs. Mariam Hassan, Mr. Jaafar Raji (Department of Physics), Mr Zainal Abidin Abbas, Mr. Ayub (Faculty of Mechanical Engineering) and Mr Said Ghani (Universiti Kebangsaan Malaysia) for their time and effort in completing my data.

Not forgetting to all lecturers, supporting staff and also the *Catalyst Technology Group* members and all the research assistants and fellow friends for their help, support, interest and valuable hints. I am particularly grateful to Department of Chemistry, Faculty of Science, Universiti Teknologi Malaysia and UTM-PTP for all facilities and financial support

Last but not least to my beloved family and friends, and especially to Ahmad Zamani Ab Halim, whose patience and love enabled me to complete this research, thank you for cheering me up all the way.

ABSTRACT

Nickel oxide based catalysts have long been known as one of the most used based materials applied for various catalyst developments. Researchers nowadays are trying to emerge with a suitable method to enhance the NiO catalyst capability for the benefit of the industries. It was observed that by introducing foreign metals with an optimized condition will increase the catalyst capability. In this study, a catalyst has been successfully developed that can potentially be used for natural gas purification where CO₂ is catalytically converted to methane. A screening test was performed in the hope to find a suitable dopant for NiO catalyst. Seven chosen metals, M*; Mg, Zr, Mo, Mn, Fe, Co, and Cu, with a required addition of Pr from the lanthanide series was incorporated into NiO based catalyst in the weight ratio of (60% Ni: 30% M*: 10% Pr) and (60% Ni: 10% M*: 30% Pr). All prepared catalysts were aged for one day and calcined for 17 hours before tested for its ability to remove CO₂ using a home-built reactor. In assistance of X-ray Diffraction (XRD) and X-ray Photoelectron Spectroscopy (XPS) analysis, Scanning Electron Microscopy (SEM), nitrogen adsorption, single point BET and Fourier Transformed Infra Red analysis (FTIR) were also carried out to reinforce the results. It was found that the incorporation of Co and Pr enhances the catalytic performance by full removal of CO₂ as well as producing methane at a low temperature of 330°C. Optimization on the ratio was carried out and was catalytically tested. From the characterization of the best catalyst, the XRD results showed that the catalyst formed individual phases of NiO, Co₃O₄ and PrO₂, while SEM assigned the presence of small particles that homogeneously distributed. The study was continued using support for the Ni/Co/Pr catalyst, whereby three supports were chosen; alumina beads (Al₂O₃), molecular sieve (Na₁₂[(AlO₂)₁₂]5SiO₂ · x H₂O), and cordierite (2MgO-2Al₂O₃-5SiO₂). Adsorption and impregnation method was used in coating the catalyst onto the support. Verifications have been made to optimize the preparation conditions; catalyst loading, time of dipping, ratio of catalyst, calcination temperature, and addition of binder. Results showed the most favorable support for Ni/Co/Pr catalyst was cordierite. From the catalytic activity, the optimum catalyst ratio for the supported catalyst was 60:35:5, and the best possible catalyst loading onto the cordierite is approximately 25 %. The optimum calcination temperature was at 400°C for 17 hours as concluded from the XRD analysis. However as the conversion of CO₂ to methane was extended for another 10 hours on stream test, it appeared that the catalytic performance declined. The decrease from a maximum of a 100 % of CO₂ conversion to 60 % conversion gave a lot of impact. From the XPS study it was found that throughout the stages of catalytic testing, the oxidation state of the individual phases changed from Ni²⁺ to Ni³⁺, and from mixture of Co²⁺ and Co³⁺ to completely Co²⁺. This finding was backed up by XRD analysis that also confirmed the changing of oxidation state. The changing of oxidation state in metal in supported catalyst resulted in rapid deactivation of catalytic performance that shortened the life span of the catalyst. The performance of the catalyst also declined as it was exposed to H₂S.

ABSTRAK

Mangkin yang berasaskan nikel oksida telah lama digunakan sebagai bahan asas di dalam pelbagai kaedah pemangkinan. Para penyelidik masa kini sedang mencuba untuk mencari kaedah yang sesuai untuk meningkatkan keupayaan mangkin NiO untuk digunakan di sektor industri. Di dalam kajian ini, satu mangkin telah dihasilkan di mana ia berpotensi untuk digunakan dalam penyulingan gas asli; CO₂ akan bertukar kepada metana dengan bantuan mangkin. Kaedah cubajaya digunakan untuk mencari bahan pendop yang sesuai untuk mangkin NiO. Tujuh logam terpilih, M*; Mg, Zr, Mo, Mn, Fe, Co, dan Cu, dan bahan pendopan yang wajib, Pr dari unsur lantanida telah dimasukkan bersama mangkin NiO di dalam nisbah berat (Ni 60%: M* 30%: Pr 10%) dan (Ni 60%: M* 10%: Pr 30%). Semua mangkin yang telah disediakan telah dikeringkan selama sehari dan dikalsin selama 17 jam sebelum keupayaan menyingkirkan CO₂ diuji menggunakan reaktor buatan sendiri. Selain daripada analisis pembelauan sinar X (XRD), dan spektroskopi elektron sinar X (XPS), analisis mikroskopi elektron (SEM), penyerapan gas nitrogen (NA), BET dan analisis infra merah (FTIR) juga telah dilakukan untuk memperkukuhkan lagi keputusan ujian. Ujian mendapati dengan penambahan Co dan Pr dapat meningkatkan keupayaan mangkin untuk menyingkirkan CO₂ sepenuhnya dan menghasilkan metana pada suhu terendah 330°C. Pengoptimuman nisbah logam telah dibuat dan diuji secara mangkin. Daripada pencirian mangkin terbaik, keputusan analisa XRD menunjukkan mangkin membentuk fasa individu NiO, Co₃O₄ dan PrO₂, manakala SEM mengesahkan pembentukan saiz zarah kecil yang sekata. Penyelidikan diteruskan dengan menggunakan bahan penyokong yang terpilih alumina (Al₂O₃), penapis molekul (molecular sieve, Na₁₂[(AlO₂)₁₂]5SiO₂.xH₂O), dan kordierit (2MgO-2Al₂O₃-5SiO₂). Kaedah penyerapan dan pengisitepuan digunakan untuk menyalut mangkin pada bahan penyokong. Pengenalpastian dilakukan untuk mencari keadaan optima bagi penyediaan mangkin; peratusan kandungan mangkin, masa celupan, nisbah logam dalam mangkin, suhu pengkalsinan, dan penambahan bahan ikatan. Keputusan menunjukkan bahan penyokong yang paling sesuai bagi mangkin Ni/Co/Pr adalah kordierit. daripada ujian pemangkinan, nisbah mangkin yang optima bagi mangkin berpenyokong adalah 60:35:5, dan peratusan kandungan mangkin yang paling baik adalah sebanyak 25 %. Suhu kalsin optima adalah suhu 400°C selama 17 jam, dan ia disokong oleh keputusan daripada XRD. Namun begitu apabila ujian penukaran CO₂ kepada metana dilanjutkan kepada 10 jam tanpa henti, keupayaan mangkin semakin menurun. Penurunan daripada 100 % penukaran CO₂ kepada 60 % telah memberi impak yang besar. Daripada analisa XPS, ia mendapati bahawa semasa peringkat ujian pemangkinan, nombor pengoksidaan bagi fasa individu telah berubah daripada Ni²⁺ kepada Ni³⁺, dan daripada campuran Co²⁺ dan Co³⁺, kepada Co²⁺ sepenuhnya. Perubahan ini juga dibuktikan daripada XRD yang mengesahkan perubahan nombor pengoksidaan. Perubahan nombor pengoksidaan logam pada mangkin berpenyokong telah menyebabkan penurunan mendadak kepada keupayaan mangkin dan memendekkan jangka hayatnya. Keupayaan mangkin menyingkirkan CO₂ juga menurun apabila ia didedahkan kepada H₂S.

TABLE OF CONTENTS

CHAPTER	TITLE	PAGE
	DECLARATION	ii
	DEDICATION	iii
	ACKNOWLEDGEMENTS	iv
	ABSTRACT	v
	ABSTRAK	vi
	TABLE OF CONTENTS	vii
	LIST OF TABLES	xiv
	LIST OF FIGURES	xvii
	LIST OF SYMBOLS AND ABBREVIATIONS	xxiii
	LIST OF APPENDICES	xxv
CHAPTER 1	INTRODUCTION	1
	1.1 Natural Gas	1
	1.2 Current natural gas purification system	4
	1.2.1 Wet Scrubber system	5
	1.2.2 Membrane separation system	6
	1.2.3 Solvent system	7
	1.2.4 Catalytic conversion system	8
	1.3 Problem statement	9
	1.4 Research objectives	9
	1.5 Scope of research	10
CHAPTER 2	LITERATURE REVIEW	11
	2.1 Nickel based catalyst	11
	2.2 Dopants contribution towards the catalyst activity	14

2.3	Metal oxide as promoters	15
2.3.1	Catalysis by magnesium oxide	15
2.3.2	Catalysis by zirconium oxide	17
2.3.3	Catalysis by molybdenum oxide	19
2.3.4	Catalysis by manganese oxide	21
2.3.5	Catalysis by cobalt oxide	22
2.3.6	Catalysis by iron oxide	25
2.3.7	Catalysis by copper oxide	27
2.4	Addition of rare earth elements as dopants	29
2.4.1	Catalysis by praseodymium oxide	30
2.5	Supported catalyst	31
2.5.1	Different forms of support	33
2.5.1.1	Honeycomb monoliths	33
2.5.1.2	Bead catalysts	36
2.5.1.3	Molecular sieves	37
CHAPTER 3	EXPERIMENTAL	40
3.1	Synthesis of the catalyst	40
3.1.1	Preparation of unsupported catalyst	40
3.1.2	Preparation of supported catalyst	42
3.2	Catalytic performance	45
3.2.1	Experimental set-up	45
3.2.2	Catalytic test	47
3.2.3	Fourier Transformed Infra Red analysis (FTIR)	48
3.3	Characterization of catalyst	49
3.3.1	X-Ray Diffraction (XRD)	50
3.3.2	X-Ray Photoelectron Spectroscopy (XPS)	51
3.3.3	Scanning Electron Microscopy (SEM) and Energy Dispersive X-ray Analysis (EDX)	55
3.3.4	Nitrogen gas Adsorption (pore texture analysis)	56
3.3.5	Single Point BET analysis	58
3.3.6	Fourier Transform Infrared Spectroscopy (FTIR)	60

CHAPTER 4	CATALYTIC ACTIVITY, MEASUREMENTS AND CHARACTERIZATION OF UNSUPPORTED CATALYST	62
4.1	Catalytic activity measurements	62
4.1.1	Addition of Mg^{2+}	64
4.1.2	Addition of Zr^{4+}	65
4.1.3	Addition of Mo^{6+}	66
4.1.4	Addition of Mn^{3+}	68
4.1.5	Addition of Co^{2+}	69
4.1.6	Addition of Fe^{3+}	70
4.1.7	Addition of Cu^{2+}	72
4.1.8	Comparison of Ni/M*/Pr catalyst with the ratio of 6:10:30 and 6:30:10 (M=Mg, Zr, Mo, Mn, Co, Fe, andCu)	73
4.1.9	Catalytic activity measurements of unsupported Ni/Co/Pr catalyst in various ratios of elemental compositions	74
4.1.10	Comparison of unsupported Ni/Co/Pr catalyst with unsupported Ni/Pr catalyst	76
4.1.11	Life span of the unsupported Ni/Co/Pr catalyst	76
4.2	Characterization	77
4.2.1	X-ray diffraction analysis (XRD)	78
4.2.1.1	XRD analysis on Ni/Mg/Pr catalyst with different ratios	78
4.2.1.2	XRD analysis on Ni/Fe/Pr catalyst with different ratios	80
4.2.1.3	XRD analysis on Ni/Co/Pr catalyst with different ratios	81
4.2.1.4	XRD on Ni/Co/Pr(60:35:5) catalyst at different calcination temperatures	83
4.2.2	Scanning electron microscopy analysis (SEM)	85
4.2.3	Energy Dispersive X-ray analysis(EDX)	86
4.2.4	Nitrogen gas Adsorption analysis (NA)	87

4.2.5	Single point BET analysis	90
4.2.5.1	Ni/M*/Pr with the ratio of 60:10:30 (M = Mg, Zr, Mo, Mn, Co, Fe, and Cu)	90
4.2.5.2	Ni/M*/Pr with the ratio of 60:30:10 (M = Mg, Zr, Mo, Mn, Co, Fe, and Cu)	91
4.2.5.3	Comparison of unsupported Ni/Co/Pr (60:35:5) with Ni/Pr (60:40) and Ni/Co (60:40) catalyst	93
4.2.6	Fourier Transformed Infra-Red analysis (FTIR)	93
CHAPTER 5	CATALYTIC ACTIVITY, MEASUREMENTS AND CHARACTERIZATION OF SUPPORTED CATALYST	96
5.1	Catalytic activity measurements	96
5.1.1	Comparison of Ni/Co/Pr catalyst performance on various supports	97
5.1.2	Comparison of cordierite supported Ni/Co/Pr catalyst with various catalyst elemental ratios	98
5.1.3	Comparison of cordierite supported Ni/Co/Pr catalyst with various catalyst loading percentages	99
5.1.4	Comparison of cordierite supported Ni/Co/Pr catalyst with various calcination temperatures	101
5.1.5	Comparison of cordierite supported Ni/Co/Pr catalyst with addition of washcoat	102
5.1.6	Comparison of Ni/Co/Pr (60:35:5) catalyst with Ni/Pr (60:40) catalyst	103
5.1.7	Life span of cordierite supported Ni/Co/Pr catalyst	104
5.1.8	Poisoning of cordierite supported Ni/Co/Pr catalyst	105
5.2	Characterization	106
5.2.1	X-ray diffraction analysis (XRD)	106

5.2.1.1	Ni/Co/Pr (60:35:5) catalyst supported onto alumina bead	107
5.2.1.2	Ni/Co/Pr (60:35:5) catalyst supported onto molecular sieve	108
5.2.1.3	Ni/Co/Pr (60:35:5) catalyst supported onto cordierite	109
5.2.1.4	Comparison of cordierite supported Ni/Pr catalyst (60:40) before and after the catalytic test	112
5.2.1.5	Comparison of Ni/Co/Pr catalyst with zirconium as binder before and after the catalytic test	113
5.2.2	X-ray Photoelectron Spectroscopy analysis (XPS) on series of cordierite supported Ni/Co/Pr catalyst at different stages of catalytic tests	114
5.2.2.1	Surface composition of Ni (2p) in cordierite supported Ni/Co/Pr catalyst at different stages of catalytic tests	115
5.2.2.2	Surface composition of Co (2p) in cordierite supported Ni/Co/Pr catalyst at different stages of catalytic tests	118
5.2.2.3	Surface composition of Pr (2p) in cordierite supported Ni/Co/Pr catalyst at different stages of catalytic tests	120
5.2.2.4	Surface composition of Mg (2p) in cordierite supported Ni/Co/Pr catalyst at different stages of catalytic tests	120
5.2.2.5	Surface composition of Al (2p) in cordierite supported Ni/Co/Pr catalyst at different stages of catalytic tests	123

5.2.2.6	Surface composition of Si (2p) in cordierite supported Ni/Co/Pr catalyst at different stages of catalytic tests	125
5.2.2.7	Surface composition of O (1s) in cordierite supported Ni/Co/Pr catalyst at different stages of catalytic tests	127
5.2.2.8	Catalyst composition and carbon contamination in cordierite supported Ni/Co/Pr catalyst at different stages of catalytic tests	130
5.2.3	Scanning electron microscopy analysis (SEM)	131
5.2.4	Energy Dispersive X-ray Analysis (EDX)	134
5.2.4.1	EDX of alumina bead supported Ni/Co/Pr catalyst with the ratio of 60:35:5	135
5.2.4.2	EDX of molecular sieve supported Ni/Co/Pr catalyst with the ratio of 60:35:5	136
5.2.4.3	EDX of cordierite supported Ni/Co/Pr catalyst with the ratio of 60:35:5	137
5.2.5	Nitrogen gas Adsorption analysis (NA)	138
5.2.6	Single Point BET analysis	141
5.2.6.1	Ni/Co/Pr (60:35:5) catalyst with different supports	141
5.2.6.2	Comparison of cordierite supported Ni/Co/Pr (60:35:5) with Ni/Pr (60:40) and Ni/Co (60:40) catalyst	142
5.2.7	Fourier Transformed Infra-Red analysis (FTIR)	143
CHAPTER 6	CONCLUSIONS AND SUGGESTIONS FOR FURTHER STUDY	146
6.1	Conclusions	146

6.2	Suggestions for further study	148
	REFERENCES	149
	APPENDICES	
	APPENDIX A	174
	APPENDIX B	175
	APPENDIX C	178
	APPENDIX D	184

LIST OF TABLES

TABLE NO.	TITLE	PAGE
1.1	Chemical composition in crude natural gas in weight percent	4
3.1	Parameters for catalytic activity measurements	47
3.2	Spectroscopic notation used in XPS	52
3.3	Classification of infrared radiation	60
4.1	Positions of the characteristic infrared stretching bands for CO ₂ , CO, CH ₄ , and OH	63
4.2	Average particle size calculated from SEM for unsupported Ni/Co/Pr catalyst in the ratio of 60:35:5	85
4.3	Elemental composition of unsupported Ni/Co/Pr catalyst (60:35:5)	86
4.4	Nitrogen gas adsorption analysis for unsupported Ni/M*/Pr catalyst in the ratio of 60:35:5. (M = Mg, Fe, Co).	87
4.5	Types of BET isotherms and porosity for unsupported Ni/M*/Pr catalyst. (M = Mg, Fe, and Co).	88
4.6	Summary of type of hysteresis and shape of pores for unsupported Ni/M*/Pr catalyst. (M = Mg, Fe, and Co).	90
4.7	Surface area of unsupported Ni, Ni/Pr (60:40), and Ni/M*/Pr catalyst (60:10:30) before and after catalytic test. (M = Mg, Zr, Mo, Mn, Co, Fe, and Cu)	91
4.8	Surface area of unsupported Ni, Ni/Pr (60:40), and Ni/M*/Pr catalyst (60:30:10) before and after catalytic test (M = Mg, Zr, Mo, Mn, Co, Fe, and Cu)	92

4.9	BET surface area of unsupported Ni/Co/Pr (60:35:5) catalyst with Ni/Pr (60:40) and Ni/Co (60:40) catalyst	93
5.1	Parameters obtained by deconvolution of XPS spectra for Ni (2p) peaks in Ni/Co/Pr catalyst material	116
5.2	Parameters obtained by deconvolution of XPS spectra for Co (2p) peaks in Ni/Co/Pr catalyst material	118
5.3	Mass percentage obtained by deconvolution of XPS spectra for Pr (2p) peaks in Ni/Co/Pr catalyst material	120
5.4	Parameters obtained by deconvolution of XPS spectra for Mg (2p) peaks in Ni/Co/Pr catalyst material	121
5.5	Parameters obtained by deconvolution of XPS spectra for Al (2p) peaks in Ni/Co/Pr catalyst material	123
5.6	Parameters obtained by deconvolution of XPS spectra for Si (2p) peaks in Ni/Co/Pr catalyst material	125
5.7	Parameters obtained by deconvolution of XPS spectra for O (1s) peaks in Ni/Co/Pr catalyst material	128
5.8	Mass percentage of the catalyst obtained by deconvolution of XPS spectra in Ni/Co/Pr catalyst material	130
5.9	Mass percentage of carbon contamination by deconvolution of XPS spectra for C (2p) peaks in Ni/Co/Pr catalyst material	131
5.10	Average particle size calculated from SEM for Ni/Co/Pr catalyst in the ratio of 60:35:5 with various supports	134
5.11	Elemental composition of alumina bead supported Ni/Co/Pr catalyst (60:35:5)	135
5.12	Elemental composition of molecular sieve supported Ni/Co/Pr catalyst (60:35:5)	137
5.13	Elemental composition of cordierite supported Ni/Co/Pr catalyst (60:35:5)	138
5.14	Nitrogen gas adsorption analysis for supported Ni/Co/Pr catalyst in the ratio of 60:35:5 with different supports	139

5.15	Types of BET isotherms and porosity for supported Ni/Co/Pr (60:35:5) catalyst by various supports	140
5.16	Summary of type of hysteresis and shape of pores for supported Ni/Co/Pr (60:35:5) catalyst by various supports	141
5.17	BET Surface area of blank support (without catalyst), and supported catalyst before and after catalytic test	141
5.18	BET surface area of cordierite supported Ni/Co/Pr (60:35:5) catalyst with Ni/Pr (60:40) and Ni/Co (60:40) catalyst	143

LIST OF FIGURES

FIGURE NO.	TITLE	PAGE
1.1	Natural Gas Consumption by Region 1970-2025	2
1.2	Diagram of complete scrubber process	6
1.3	Diagram of basic membrane separation	7
2.1	Potential interactions of CO ₂ with MgO surface sites	16
3.1	Steps in adsorption of the catalyst	43
3.2	Schematic diagram of home built micro reactor	46
3.3	Packing arrangements of component in the sample tube	47
3.4	Schematic diagram of KBr window cell in the alignment with the FTIR beam	49
3.5	X-rays scattered by atoms in an ordered lattice interfere constructively in directions given by Braggs Law	50
3.6	Photoemission and the Auger process. Left: an incident X-ray photon and a photoelectron emitted.	52
3.7	Block diagram of a photoelectron spectrometer	54
3.8	IUPAC Classifications of Gas Adsorption Isotherms	57
3.9	IUPAC Classification of hysteresis	58
4.1	Representative of the FTIR spectra for the CO ₂ decreasing peak and formation of CH ₄ peak in the catalytic testing with the increase of temperature	63
4.2	Percentage of CO ₂ removal (line chart) and CH ₄ detected (bar chart) for Ni/Mg/Pr catalyst with the ratio of 60:10:30 and 60:30:10, and Ni/Mg 60:40 versus temperature from 25-500 °C	64

4.3	Percentage of CO ₂ removal (line chart) and CH ₄ detected (bar chart) for Ni/Zr/Pr catalyst with the ratio of 60:10:30 and 60:30:10, and Ni/Zr 60:40 versus temperature from 25-500 °C	66
4.4	Percentage of CO ₂ removal (line chart) and CH ₄ detected (bar chart) for Ni/Mo/Pr catalyst with the ratio of 60:10:30 and 60:30:10, and Ni/Mo 60:40 versus temperature from 25-500 °C.	67
4.5	Percentage of CO ₂ removal (line chart) and CH ₄ detected (bar chart) for Ni/Mn/Pr catalyst with the ratio of 60:10:30 and 60:30:10, and Ni/Mn 60:40 versus temperature from 25-500 °C	69
4.6	Percentage of CO ₂ removal (line chart) and CH ₄ detected (bar chart) for Ni/Co/Pr catalyst with the ratio of 60:10:30 and 60:30:10, and Ni/Co 60:40 versus temperature from 25-500 °C.	70
4.7	Percentage of CO ₂ removal (line chart) and CH ₄ detected (bar chart) for Ni/Fe/Pr catalyst with the ratio of 60:10:30 and 60:30:10, and Ni/Fe 60:40, versus temperature from 25-500 °C	71
4.8	Percentage of CO ₂ removed (line chart) and CH ₄ detected (bar chart) for Ni/Cu/Pr catalyst with the ratio of 60:10:30 and 60:30:10, and Ni/Cu 60:40, versus temperature from 25-500 °C.	72
4.9	Comparison of CO ₂ removal and CH ₄ yield for Ni/M*/Pr catalyst in the ratio of (a) 60:10:30 and (b) 60:30:10. (M=Mg, Zr, Mo, Mn, Co, Fe, and Cu) at the temperature of 350 °C	74
4.10	CO ₂ elimination for Ni/Co/Pr catalyst with various ratios of Co at the temperature in the range of 30 to 500°C.	75
4.11	CO ₂ elimination for Ni/Co/Pr (60:35:5) and Ni/Pr (60:40) catalyst at the temperature in the range of 30 °C to 500°C	76

4.12	The catalytic activity of powdered Ni/Co/Pr catalyst versus number of catalytic testing	77
4.13	Diffractiongram of unsupported Ni/Mg/Pr with ratio of (a) 60:10:30 and (b) 60:30:10	79
4.14	Diffractiongram of unsupported Ni/Fe/Pr with ratio of (a) 60:10:30 and (b) 60:30:10	81
4.15	Diffractiongram of unsupported Ni/Co/Pr with ratio of (a) 60:10:30 and (b) 60:30:10	82
4.16	Diffractiongrams of unsupported Ni/Co/Pr ratio 60:35:5 catalyst calcined at different temperatures; (a) 300°C, (b) 400°C, and (c) 800°C	84
4.17	SEM micrographs of unsupported Ni/Co/Pr catalyst in the ratio of 60:35:5 (a) before and (b) after it was calcined at 400°C for 17 hours. (Magnification 1000x)	85
4.18	EDX of unsupported Ni/Co/Pr catalyst with ratio of (60:35:5)	86
4.19	BET isotherm plot of unsupported Ni/Mg/Pr catalyst in the ratio of 60:35:5	88
4.20	BET isotherm plot of unsupported Ni/Fe/Pr catalyst in the ratio of 60:35:5.	89
4.21	BET isotherm plot of unsupported Ni/Co/Pr catalyst in the ratio of 60:35:5	89
4.22	Spectra of unsupported Ni/M*/Pr (M* = Mg, Mo, Zr, Mn, Co, Fe, Cu) in the ratio of 60:30:10 after calcined at 400°C before catalytic testing	94
4.23	Spectra of unsupported Ni/M*/Pr (M* = Mg, Mo, Zr, Mn, Co, Fe, Cu) in the ratio of 60:30:10 after calcined at 400°C and after catalytic testing	95
5.1	Catalytic activity of various supported Ni/Co/Pr catalysts with the ratio of 60:35:5	97
5.2	Catalytic activity of cordierite supported Ni/Co/Pr with various ratio of elemental composition (a) 60:35:5, (b) 50:45:5, (c) 47.5: 47.5: 5, and (d) 45:50:5	98

5.3	Catalytic activity of cordierite supported Ni/Co/Pr with various catalyst loading percentage of (a) 5%, (b) 25%, and (c) 50%.	99
5.4	Catalytic activity of cordierite supported catalyst with different duration of dipping time; (a) 0.25hours, (b) 1hour, (c) 12 hours, (d) 24 hours, and (e) 48 hours	101
5.5	Catalytic activity of cordierite supported Ni/Co/Pr with various calcination temperatures (a) 400 °C, (b) 600 °C, and (c) 800 °C for 10 hours	102
5.6	Catalytic activity of cordierite supported Ni/Co/Pr with addition of (a) magnesium, and (b) zirconium as binder compared to cordierite supported Ni/Co/Pr catalyst	103
5.7	CO ₂ elimination for Ni/Co/Pr (60:35:5) and Ni/Pr (60:40) catalyst supported by cordierite from the temperature of 25 to 500°C.	104
5.8	Catalytic activity of cordierite supported Ni/Co/Pr catalyst versus number of catalytic tests	105
5.9	Catalytic activity of cordierite supported Ni/Co/Pr catalyst that has been exposed to (a) CO and (b) H ₂ S for 2 hours at 300 °C of temperature before the catalytic testing	106
5.10	Diffractiongram of alumina bead supported Ni/Co/Pr (60:35:5) catalyst	108
5.11	Diffractiongram of molecular sieve of supported Ni/Co/Pr (60:35:5) catalyst	109
5.12	Diffractiongrams of cordierite supported Ni/Co/Pr catalyst (60:35:5) at different stages of catalytic testing; (a) before catalytic test, (b) after first catalytic test (intermediate), and (c) after third catalytic test	111
5.13	Diffractiongrams of cordierite supported Ni/Pr (60:40) catalyst (a) before, and (b) after testing	112
5.14	Diffractiongrams of cordierite supported Ni/Co/Pr (60:35:5) catalyst with Zr as binder (a) before, and (b) after testing	113

5.15	XPS spectra of deconvoluted Ni (2p) for (a) unsupported Ni/Co/Pr catalyst, (b) cordierite supported Ni/Co/Pr catalyst before catalytic testing, (c) cordierite supported Ni/Co/Pr catalyst after first catalytic testing, and (d) cordierite supported Ni/Co/Pr catalyst after third testing	117
5.16	XPS spectra of deconvoluted Co (2p) for (a) unsupported Ni/Co/Pr catalyst, (b) cordierite supported Ni/Co/Pr catalyst before catalytic testing, (c) cordierite supported Ni/Co/Pr catalyst after first catalytic testing, and (d) cordierite supported Ni/Co/Pr catalyst after third testing	119
5.17	XPS spectra of deconvoluted Mg (2p) for (a) cordierite support without catalyst, (b) cordierite supported Ni/Co/Pr catalyst before catalytic testing, (c) cordierite supported Ni/Co/Pr catalyst after first catalytic testing, and (d) cordierite supported Ni/Co/Pr catalyst after third testing	122
5.18	XPS spectra of deconvoluted Al (2p) for (a) cordierite support without catalyst, (b) cordierite supported Ni/Co/Pr catalyst before catalytic testing, (c) cordierite supported Ni/Co/Pr catalyst after first catalytic testing, and (d) cordierite supported Ni/Co/Pr catalyst after third testing	124
5.19	XPS spectra of deconvoluted Si (2p) for (a) cordierite support without catalyst, (b) cordierite supported Ni/Co/Pr catalyst before catalytic testing, (c) cordierite supported Ni/Co/Pr catalyst after first catalytic testing, and (d) cordierite supported Ni/Co/Pr catalyst after third testing	126
5.20	XPS spectra of deconvoluted O (1s) for (a) cordierite support without catalyst, (b) cordierite supported Ni/Co/Pr catalyst before catalytic testing, (c) cordierite supported Ni/Co/Pr catalyst after first catalytic testing, and (d) cordierite supported Ni/Co/Pr catalyst after third testing	129
5.21	SEM micrographs of alumina bead supported Ni/Co/Pr catalyst in the ratio of 60:35:5 (a) before and (b) after it was calcined at 400°C for 17 hours. (1000x and 5000x)	132

5.22	SEM micrographs of molecular sieve supported Ni/Co/Pr catalyst in the ratio of 60:35:5 (a) before and (b) after it was calcined at 400°C for 17 hours. (Magnification 1000x and 5000x)	133
5.23	SEM micrographs of cordierite supported Ni/Co/Pr catalyst in the ratio of 60:35:5 (a) before and (b) after it was calcined at 400°C for 17 hours. (Magnification 1000x and 5000x)	134
5.24	EDX of alumina bead supported Ni/Co/Pr catalyst (60:35:5)	135
5.25	EDX of molecular sieve supported Ni/Co/Pr catalyst (60:35:5)	136
5.26	EDX of cordierite supported Ni/Co/Pr catalyst (60:35:5)	137
5.27	BET isotherm plot of alumina supported Ni/Co/Pr catalyst in the ratio of 60:35:5	139
5.28	BET isotherm plot of molecular sieve supported Ni/Co/Pr catalyst in the ratio of 60:35:5	140
5.29	BET isotherm plot of cordierite supported Ni/Co/Pr catalyst in the ratio of 60:35:5	140
5.30	FTIR spectrum of alumina bead supported Ni/Co/Pr (60:35:5) catalyst	144
5.31	FTIR spectrum of molecular sieve supported Ni/Co/Pr (60:35:5) catalyst	144
5.32	FTIR spectrum of cordierite supported Ni/Co/Pr (60:35:5) catalyst	145

LIST OF SYMBOLS AND ABBREVIATIONS

BET	-	Brunnauer, Emmett and Teller
Conv.	-	Conversion
Cu K _α	-	X-ray diffraction from Copper K energy levels Rate of Conversion (percentage)
d	-	Pore diameter
DTA	-	Differential thermal analysis
EDX		Energy Dispersive X-Ray Analysis
EDF	-	Equilibrium deposition filtration
EIA	-	Energy Information Administration
FTIR	-	Fourier Transformed Infra Red
HC	-	Hydrocarbon
IR	-	Infra red
IUPAC	-	International Union of Pure and Applied Chemistry
IWI	-	Incipient Wetness Impregnation
NA	-	Nitrogen gas adsorption
NG	-	Natural gas
NO _x	-	Nitrogen oxides
OSC	-	Oxygen Storage Capacity
P/P_o	-	Relative pressure; obtained by forming the ratio of the equilibrium pressure and vapour pressure P_o of the adsorbate at the temperature where the isotherm is measured
PDF	-	Powder Diffraction File
REO	-	Rare Earth Oxides
RT	-	Room Temperature
SEM	-	Scanning Electron Microscopy

SMSI	-	Strong Metal-Support Interaction
TG	-	Thermogravimetry
T _{LO}	-	Light-off Temperature
T _{max}	-	Maximum Conversion Temperature
TOF	-	Turnover frequency (repeated tests)
TWC	-	Three-way Catalyst
w/w %	-	Weight per weight percentage ratio.
XPS	-	X-ray Photoelectron Spectroscopy
XRD	-	X-ray Diffraction
θ	-	Half Angle of Diffracted Beam
λ	-	wavelength
ΔE_{so}	-	Spinning orbital energy

LIST OF APPENDICES

APPENDIX	TITLE	PAGE
A	Calculation of atomic weight percentage ratio of element in catalyst preparation	178
B	Calculation of the percentage for CO ₂ removal and CH ₄ yield from catalytic testing	175
C	<i>d</i> -spacing values from XRD analysis of unsupported and supported catalyst	178
D	Figures of supported catalyst with different metal loadings	184

CHAPTER 1

INTRODUCTION

1.1 Natural Gas

Natural gas is a fossil fuel that was found far below the earth's crust, much further than oil deposits, formed when organic matter (remains of plants and animals) was compressed at high pressure for a long time. It is also known as thermogenic methane. Akin to the formation of oil, the particulates were piled up with mud and other sediment on top of the other occasionally until the weight of the debris puts a great deal of pressure on the organic matter. Combining with the heat from underneath, the organic matter will breakdown and form lower carbon-carbon bonds. It may also have been formed by slow out gassing of methane from vast deep deposits dating back to the origin of our planet. The formation of methane depends on the heat, whereby the lower temperature will form oil deposits and the higher temperatures primarily form methane (Kiricsi and Guzzi, 1999).

Natural gas is a colorless and odorless in its pure form. It is combustible and has been proven to be a renewable energy source as it gives a great deal of power upon consumption (Olah and Molnar, 2003). Natural gas is the fastest growing primary energy source in the *International Energy Outlook 2004* (EIA, 2004) forecast (EIA, 2004). Consumption of natural gas worldwide is projected to increase by an average of 2.2 percent annually from 2001 to 2025, which is increase by nearly 70 percent higher than energy consumed in 2001. The projected demand is definitely

higher compared with annual growth rates of 1.9 percent for oil consumption and 1.6 percent for coal. Furthermore, the most robust growth in natural gas demand is expected among the developing nations, including Malaysia, where overall demand is projected to increase by an average of 2.9 percent per year from 2001 to 2025. Most of that increase is expected to be for daily usage of electricity generation through pipeline or in the form of liquefied natural gas (LNG).

The world natural gas reserves have generally trended upward since the mid-1970s (Figure 1.1) until now and it was proven that the developing countries accounted for virtually all in the increase in proved reserves (EIA, 2004; Radler, 2003). In 2002, Indonesia and Malaysia were the largest natural gas producers in developing Asia, exporting 1108 and 741 billion cubic feet of natural gas, respectively, and accounted for about 70 % of Asia's gas trade, both by way of pipeline (small amounts to Singapore) and as LNG (to Japan, South Korea, Taiwan and United States) (EIA, 2003).

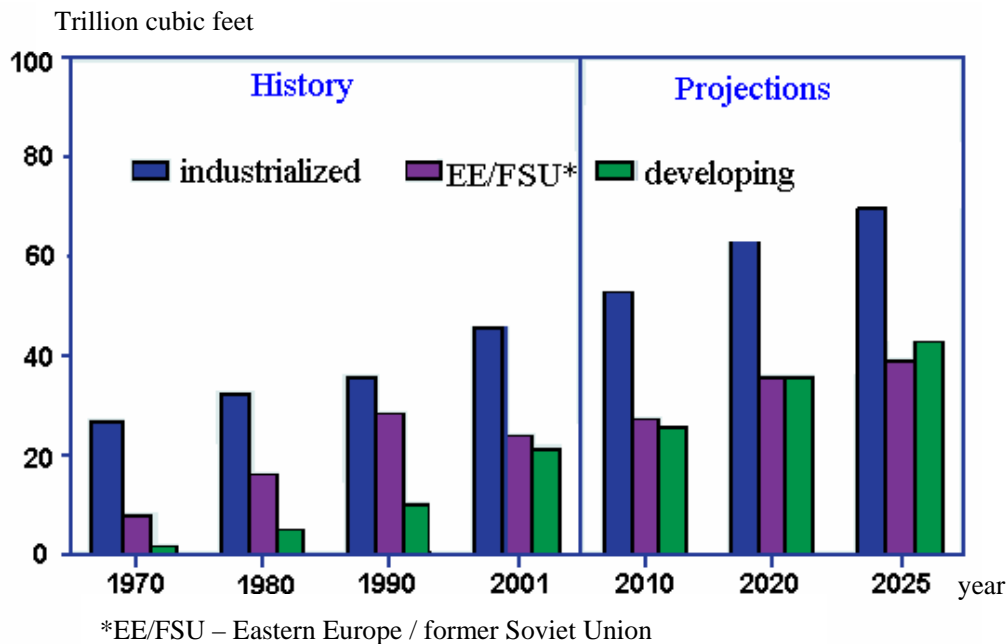


Figure 1.1 Natural Gas Consumption by Region, 1970-2025 (EIA, 2004)

Malaysia's proved gas reserves were estimated 75 million cubic feet (Radler, 2001). About 60 % of its marketed gas production is consumed domestically, three-quarters of which is used for generating electricity. Malaysia is also the region's second largest LNG exporter, accounting for 14 % of total world trade in LNG in 2002. Malaysia's reserves are mainly in eastern Malaysia, which is Sarawak and Sabah (59 %) and the rest are at the offshore east coast of Peninsular Malaysia. The largest gas field is in Miri, Sarawak. It was followed by Kota Kinabalu, Sabah.

The country is seeking ways to increase its production of natural gas. Approximately 38 % of Malaysia's reserves are under Petronas Carigali Sdn. Bhd. (Muhamad, 2001). Malaysia also has offshore fields in the South China Sea, which have been developed by Exxon Mobil (EIA, 2004). The country is currently exporting 9.2 billion cubic feet of natural gas per year to Singapore via pipeline. The Malaysia-Thailand Joint Development Authority is a joint-venture program by the two countries and now is being explored by Petronas and the Petroleum Authority of Thailand (PTT) as well as Amerada Hess and BP. Its purpose is to build a pipeline linked to a gas-fired electricity generation plant in Thailand near the Thailand's and Malaysia's boundaries, with plans for a future gas pipeline to Malaysia. Malaysia has also begun imports of Indonesian gas from Natuna offshore field through a connection to Malaysia's Duyong field pipeline (EIA, 2004) in order to position itself as Southeast Asia's gas hub.

In view of the expected growth in the demand for natural gas increasing attention is being devoted by the gas industry to upgrade of low quality of natural gas. Table 1.1 (Kiricsi and Guzzi, 1999) showed the chemical composition of Malaysian raw untreated natural gas. It is primarily consists of low density hydrocarbons (methane, ethane, propane), and impurities (CO₂, H₂S, O₂, N₂ etc.)

From the comparison of the location, it is clearly stated that Malaysian raw natural gas consists of more of the impurities; sour gas and flue gas than any other countries stated above. These impurities will lower the price of natural gas in the worldwide market and will also cause trouble for distributing them.

Table 1.1: Chemical composition in crude natural gas in weight percent (w/w %) (Olah and Molnar, 2003; Minerals and Geoscience Department of Malaysia, 2001)

Location	CH ₄	C ₂ H ₆	C ₃ H ₈	C ₄ H ₁₀	Others (CO ₂ , H ₂ S, O ₂ , N ₂)
United States	89.5	5.1	0.7	0.5	4.2
Algeria	86.9	9.0	2.6	1.2	0.3
Iran	74.9	13.0	7.2	3.1	1.8
North Sea	90.8	6.1	0.7	0.1	2.3
Malaysia	70.0	13.0	6.0	1.0	10.0

1.2 Current natural gas purification system

The major problem of having impurities in natural gas is not only it will lower the quality of natural gas, it will also affect worldwide price. High cost is needed in all the stages of providing customers with natural gas that met with US pipeline specification, which is that the natural gas must contain not more than 2 w/w% CO₂ and 4 ppm H₂S before being delivered to customers (Echterhoff and McKee, 1991). With steel pipelines as medium of transportation that easily can rust and corrode by carbonic acid from sour gas (Ertesva *et al.*, 2005; Zou *et al.*, 2005), and very long distance is involved, whereby pipelines in South East Asia are over 4000 km in length, creating complications in the computation of costs to frequently replace with new pipelines (Wybrew-Bond and Stern, 2002). That is why in view of expected growth in the demand for natural gas, increasing attention is being devoted by the gas industry to the upgrading of low-quality natural gas.

A variety of conventional separation methods are presently being used to remove the “acid gasses”, CO₂ and H₂S from crude natural gas (Abdellah *et al.*, 2003; Pei *et al.*, 2004; Vu *et al.*, 2003; Taulbee *et al.*, 1996; Hao *et al.*, 2002). These methods include gas adsorption on solid sorbents, absorption in liquid solvents, and chemical conversion.

1.2.1 Wet Scrubber system (WGS)

One of the suggestions was the use of limestone-based sorbents which is a flue gas desulphurization unit, for the removal of CO₂ from multi-component gas streams (Taulbee *et al.*, 1996). Wet scrubbers capture sulfur in flue gas to form both hydrated and slurry mixture of Ca, Ca(OH)₂ and CaSO₄. It was also been used as biotrickling filters for H₂S control in the environment (Gabriel *et al.*, 2004). An overview of the Wet Gas Scrubber system (WGS) used by one of the Malaysian NG company is in Figure 1.2 (Morris, 2002);

- The small, on-site WGS washes the flue gas removing both particulate and sulfur oxides.
- The cleaned flue gas is then exhausted to the atmosphere with residual particulate and sulphur oxides.
- Other streams entering the Wet Gas Scrubber are water and an alkali.
- A separate liquid purge stream leaves the WGS for further treatment.
- The purge stream, which contains the particulate and sulfur oxides removed from the flue gas, may either be treated in the refinery's existing wastewater treatment system or may be treated in a dedicated PTU (Purge Treatment Unit).
- The discharge from the PTU consists of earth moist solids suitable for sanitary landfill disposal and a benign liquid.

The advantages of using this method are it provides efficient chemical usage and it is also stable in low pH conditions. It does not promote scale and corrosion in the system and operates at low temperatures. However, the waste product exhibits a strong affinity for CO₂, whereby it was reacted with unsulfated Ca to form CaCO₃. Although it is able to absorb CO₂, a significant amount of waste is formed with the absorption. Furthermore, a separate disposal treatment has to be developed in order to treat the waste.

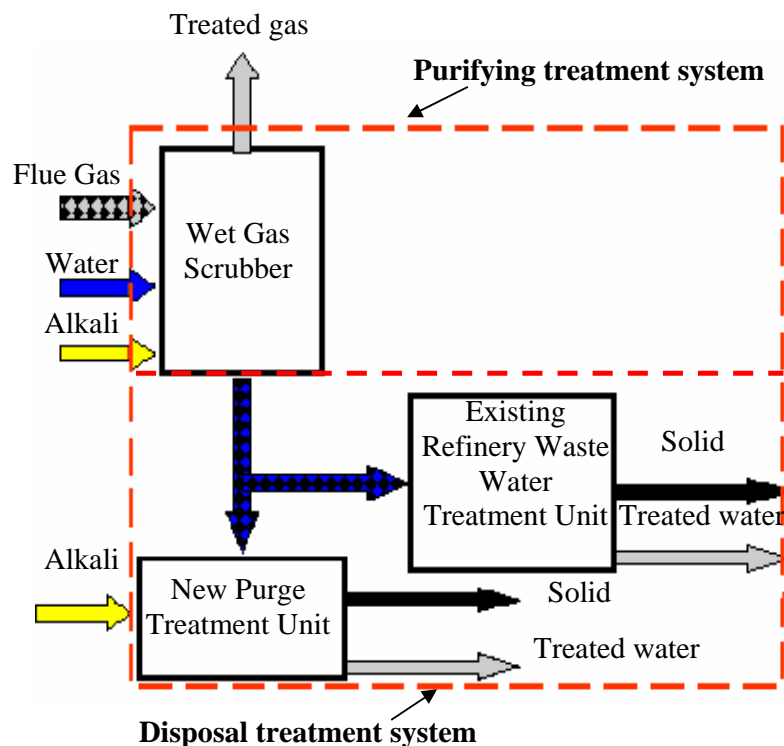


Figure 1.2 Diagram of complete scrubber process (Morris, 2002)

1.2.2 Membrane separation system

Membrane separation processes have also emerged as an alternative and offered a number of important advantages for the upgrading of crude natural gas (Abdellah *et al.*, 2003). Membrane separation involves partially separating a feed containing a mixture of two or more components by use of a semi permeable barrier (the membrane) through which one or more of the species moves faster than another or other species. As shown in Figure 1.3, the basic process of the membrane separation involves a feed mixture separated into a *retentate* (part of the feed that does not pass through the membrane, i.e., is retained) and a *permeate* (part of the feed that passes through the membrane). It was found to economically reduce the concentrations of CO_2 and H_2S whereby it require polymer membranes that exhibit high CO_2/CH_4 or $\text{H}_2\text{S}/\text{CH}_4$ selectivity, or both types of membranes.

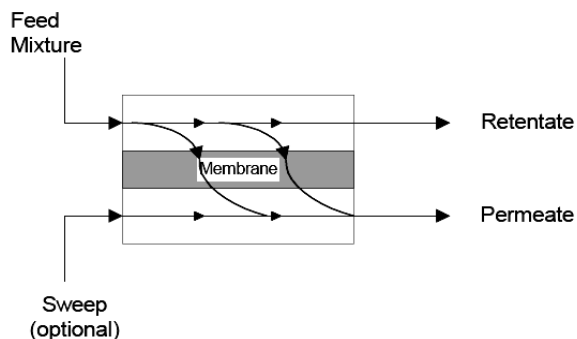


Figure 1.3 Diagram of basic membrane separation (Ali *et al.*, 2000)

Hence the issue not considered in this study is the environmental impact of the permeate product streams. These streams will contain substantial amounts of H_2S and cannot be discharged to the atmosphere. For this reason and also because of economic considerations the permeate streams will have to be treated by a suitable sulphur recovery process. The nature of this process will depend on the composition and flow rates of the permeate streams (Hao *et al.*, 2002).

1.2.3 Solvent system

Traditionally the preferred acid component removal routes were based on various amine-based or mixed solvent processes for relevant sulphur component removal, followed with drying of the gas by molecular sieves. Alternately, amine processes have been selected which did not remove the mercaptants, the latter being achieved by the molecular sieves or a physical solvent processes. These techniques have been adapted by oil and gas companies that are treating their feed gas which contains CO_2 , H_2S and other organic sulphur components (Van der Graaf and Klinkenbijn, 2003).

The patented research by Triplett and Brauer (1970) has included the purification of petroleum along with natural gas. The process provides methods for dissolution of the petroleum products followed by displacement through the subterranean formation from one or more injection wells to one or more production wells. The process provides for downhole heating of the liquid solvent in each

injection well at the time the liquid solvent flows into the formation from the injection well. The liquid solvent is heated through the use of heat generated by radioactive waste material in general.

Processes such as this are mainly to be used when the petroleum is of low gravity and/or the formation is of low porosity, so that the petroleum has poor flow characteristics through the formation. Since the solvent dissolves the petroleum, and both the solvent and the solvent-petroleum solution have relatively low gravities and viscosities, flow through the formation is improved. But the problem is that another treatment has to be conducted in order to separate the solvent from the petroleum.

1.2.4 Catalytic conversion system

Then the researchers turn to the most promising alternative catalytic conversion. The research interest in the catalytic reforming of CO₂ to methane has been increasing. The hydrogenation of CO₂ to methane is potentially an important reaction. The reaction of CO hydrogenation into methane is a particularly favorable example for applying these techniques since it combines fast steps such as H₂ and CO activation (Agnelli *et al.*, 1998), affordable system as only the catalyst has to be maintained and it possibly can be recycled, and environmental friendly as it does not permeate any toxic gasses during reaction into the air.

The basic reaction of methanation can be considered either as a target reaction for producing methane for further chemical use or for burning as an auxiliary heat source or as a detrimental route when higher hydrocarbons and/or oxygenates are targeted such as those for the Fischer-Tropsch process or for methanol or higher alcohols syntheses (Agnelli and Mirodatos, 2000).

Methanation can be accomplished by applying heterogeneous metal oxide catalysts. Due to the high activity of rhodium and ruthenium catalysts most of the recent investigation for methanation of CO₂ have been carried out using supported Rh and Ru catalyst (Kudo and Komatsu, 1999a; 1999b). Besides commonly used

supported metal catalysts, amorphous alloys have attracted great interest as catalyst and catalyst precursors (Yamasaki *et al.*, 1997; Habazaki *et al.*, 1998). Ni is also well-known catalyst that is suitable for hydrogenation and popular reported for its low price (Aksoylu and Onsan, 1997; Yamasaki *et al.*, 1997). It possesses high activity and selectivity for CO₂ elimination, while coke deposition, which deactivates Ni catalyst and blocks the reactor, is the main problem. A lot of promoters have been reported for Ni catalyst to depress coke deposition, increase catalytic activity, and also to lower the elimination temperature so that all the CO₂ will be removed at lowest temperature possible.

1.3 Problem statement

Natural gas, typically methane, is frequently contaminated with moisture, nitrogen gas, carbon dioxide and other hydrocarbons. At some point in the extraction, transportation or treatment stages, it is important that these impurities and extraneous hydrocarbon molecules be removed or separated. Nickel based catalysts are generally considered as reference methanation catalysts, able to work efficiently in the temperature and pressure ranges of 400 to 500°C and 1000–7000 kPa (Agnelli and Mirodatos, 2000). Deactivation processes remain, however, as the main drawback encountered for this reaction. The present work was devoted to study a suitable promoter needed towards finding an affordable novel catalyst for CO₂ elimination that is high in activity, stability and selectivity. The nickel based catalyst was doped with foreign metal oxide and added with Pr. The best promoted nickel catalyst was then supported on various supports to obtain the most fitting supported catalyst towards CO₂ methanation.

1.4 Research objectives

The objectives of this research are as follows;

1. To convert CO₂ to methane using catalytic conversion of CO₂ to fuel gas.
2. To observe the effect of different mixtures of metal oxides in different ratios towards CO₂ removal.
3. To modify the catalyst to enhance the capability in catalytic activity, selectivity and durability using affordable metals to lower the cost.
4. To study the suitability and potential of mixed oxide catalyst onto different forms of support for commercialization.

1.5 Scope of research

In this research, Ni/Pr catalyst was added with selected foreign metals, M* (M* = Mg, Mo, Zr, Mn, Fe, Co, Cu), in different ratios to compose a mixed metal oxide catalyst, Ni/M/Pr. The catalyst was tested in the hope to remove CO₂ with the presence of H₂ resulting in CO₂ hydrogenation. The best unsupported catalyst was then supported on various supports to determine its compatibility between the catalyst and support and to find out its physical changes as it was put through catalytic testing. The reducibility and characteristics of the Ni based catalysts were tested by means of FTIR for catalytic activity. XRD analysis was carried out to determine phase or structural changes and it was complimented by XPS analysis that determined the oxidation state. Meanwhile, SEM, nitrogen adsorption and single point BET analysis were carried out to verify the changes in surface area and pore size of the catalyst.